Journal of Photochemistry & Photobiology, A: Chemistry 444 (2023) 114987

Contents lists available at ScienceDirect

Journal of Photochemistry & Photobiology, A: Chemistry

journal homepage: www.elsevier.com/locate/jphotochem

Exploring the nonlinear optical limiting activity of *para*-aminobenzoic acid by experimental and DFT approach

Shradha Lakhera [a], Meenakshi Rana [a,*], Kamal Devlal [a], Shruti Sharma [b], Papia Chowdhury [b], Vivek Dhuliya [c], Sagar Panwar [c], L.P. Purohit [c], A. Dhanusha [d], T.C. Sabari Girisun [d]

[a] Department of Physics, School of Sciences, Uttarakhand Open University, Haldwani 263139, Uttarakhand, India
[b] Department of Physics and Materials Science and Engineering, Jaypee Institute of Information Technology, Noida 201309, Uttar Pradesh, India
[c] Department of Physics, Gurukula Kangri (Deemed to be University), Haridwar 249404, Uttarakhand, India
[d] Nanophotonics Laboratory, Department of Physics, Bharathidasan University, Tiruchirappalli, Tamil Nadu 620024, India

ARTICLE INFO

Keywords:
Density functional theory
Nonlinear optics
para-Aminobenzoic acid
Optical limiting
Hyperpolarizability

ABSTRACT

The present study accounts for the nonlinear optical behavior of *para*-aminobenzoic acid. The intramolecular charge transfer was established using electrostatic potential and Hirshfeld's surfaces. The fingerprint plots identified that the bonds associated with the functional groups of *para*-aminobenzoic acid (amino and carboxyl) have major contributions to the total intramolecular charge transfer. It was observed that the *para*-aminobenzoic acid gave a broad absorption spectrum between 240 and 310 nm wavelength experimentally as well as computationally. From Tauc's plot, the obtained direct band gap of *para*-aminobenzoic acid is 3.66 eV. The vibrational peaks of experimental FT-IR spectra were also found similar to the peaks observed in computational FT-IR. Moreover, high-frequency peaks were observed for the associated functional groups. The first-order hyperpolarizability of *para*-aminobenzoic acid was computed around 29.99×10^{-30} esu. We derived from the open-aperture Z-scan data that the *para*-aminobenzoic acid exhibits strong reverse saturable absorption. The positive value of the nonlinear absorption coefficient established the potential application of *para*-aminobenzoic acid in strong multi-photon absorption. Theoretical fit and intensity dependent Z-scan experiment confirm the occurrence of excited absorption (or) sequential two-photon absorption. The present study promises *para*-aminobenzoic acid for optical limiting applications.

1. Introduction

The new novel nonlinear optical (NLO) materials have led to a new revolution in the field of optical storage, telecommunications, medical diagnosis, second harmonics, ultrafast response time, high internal quantum efficiency, high damage threshold, low dielectric constants, low operating voltage, etc [1–4]. The potential applications of these materials are not only constrained in these fields only but also in the field of optical limiting [5]. Due to having a high laser damage threshold, these materials are perfect for fabrication of the devices that provide protection from high-frequency lasers to the human eye [6]. Even, such materials are nowadays been employed for the fabrication of the eye-lens that will resist high-intensity field lines from entering and damaging the human vision [7]. The day-to-day increasing demands of such materials have raised a rapid growth of highly potent NLO active materials.

The research industry is very dynamic as its parameters and tools undergo development in order to achieve precision and accuracy. Experimental researchers face numerous challenges in having a proper plan to follow, and the biggest insecurity is either the followed procedure will be successful in yielding the desirable outputs [8]. Density functional theory (DFT), however, is a tool that is proven smooth enough to reduce the efforts of researchers. Thus, DFT is a proven theory that helps in the pre-estimation of the preferred results and is widely followed by researchers [9]. In the present study, the DFT was used for the calculation of the parameters that immensely affect the NLO activity of the materials. In order to be non-linearly polarized, the compounds must possess intramolecular charge transfer (ICT) [10]. This is possible when the compound has some donor (acceptor) group to lose (gain) electrons [11]. The computed spectral results obtained from DFT can be not only useful in the selection of the perfect compounds for experimental work but also in the comparison and validation of the

* Corresponding author.
E-mail address: mrana@uou.ac.in (M. Rana).

https://doi.org/10.1016/j.jphotochem.2023.114987
Received 20 April 2023; Received in revised form 14 June 2023; Accepted 25 June 2023
Available online 26 June 2023
1010-6030/© 2023 Elsevier B.V. All rights reserved.

experimental spectral results. The DFT tools also allow one to calculate the polarizability parameters that define the NLO activity of the compounds. There are numerous options, where a researcher of NLO can switch. Hydrocarbons, dyes, plant phytochemicals, aromatic compounds, quantum dots, polymers, conjugated molecules, fullerenes, perovskites, halogenated compounds, etc., are a few categories that provide a wide domain of structures that can be used for the synthesis of NLO active materials [12–14]. Varieties of the compounds consist of active nucleophilic and electrophilic constituents that create the ideal environment for shifting the charge cloud from electron-excess moieties towards electron-deficient moieties [15]. These intramolecular interactions lead to ICT within the materials which is key to NLO activity [16]. It was mostly observed that the compounds having electrophilic and nucleophilic moieties showed better values for dipole moment, hyperpolarizability, and susceptibility [17]. Many natural dyes were also used for the synthesis of the NLO crystals. It was observed that the availability of $–NH_2$ and –COOH groups in the molecules leads to a massive transfer of the charge cloud that shows the ICT process [18]. Amino acids and their derivatives were widely being explored for the production of third-order NLO susceptibility and harmonics generation [2].

Aminobenzoic acids and their derivatives have been extensively used for various applications such as light-emitting diodes, chemical sensors, junction transistors, corrosion inhibitors, etc [19]. The aminobenzoic acids show ultimate charge transport activities due to the presence of $–NH_2$ and –COOH groups which attain intramolecular interactions [20]. Thus, the availability of active electron-donating and electron-withdrawing moieties make the aminobenzoic acids suitable candidates for NLO applications. The optical limiting behavior of Isonicotinamide bis-p-aminobenzoic acid was studied by A. Vijaylakshmi and team by developing the crystal of the compound in methanol [21]. The relative optical transmittance for this crystal was found to be 58% [21]. The NLO behavior of the 2-amino-4,6-dimethylpyrimidine benzoic acid was established by Lasalle and the team [22]. The Z-scan experiment done on 2-amino-4,6-dimethylpyrimidine benzoic acid gave the negative value for the non-linear refractive index showing the optical limiting behavior of the crystal [22]. Studies were also reported where thin films of the derivatives of aminobenzoic acids 4-(ferrocenylmethylimino)-2-hydroxy-benzoic acid were grown and then employed for NLO and other optoelectronic applications [23]. Essential amino acids are proven efficient NLO materials. An efficient amino acid NLO single crystal L-phenylalanine–benzoic acid was studied by S. Tamilselvan and the team [24]. The laser damage threshold of a single crystal developed by the slow evaporation technique has been found to be 6.5 GW/cm^2 [24]. The sample was thermally stable up to 134C. T. Bharanidharan and his team worked on the crystal growth and optical limiting behavior of N-methyl urea benzoic acid and explored high optical transmittance of 85% [25]. The property of reverse saturable absorption of 4-nitrophenol 4-aminobenzoic acid monohydrate by open aperture Z-scan technique was accounted by P. Karuppasamy and their co-workers [26].

Open aperture mode Z-scan experiment is used to determine the nonlinear absorption and predict the material's suitability for optical limiting applications. The present study accounts for the optical limiting behavior and third-order NLO activity of *para*-aminobenzoic acid (PABA) by experimental as well as computational approaches. The computational study was done using density functional theory (DFT). The absorption spectra was obtained by both experimental and simulated means to account for the electronic activity of PABA. The vibrational study was accounted for PABA using experimental and simulated Fourier-transform infrared spectroscopy (FT-IR) [27,28]. Chemical reactivity and charge transport activity were predicted by computational tools like molecular electrostatic potential (MEP) surfaces, Hirshfeld surfaces, 2-D fingerprint plots, Van der Waals surfaces, and counterplots [29,30]. The excitation of the electrons was studied by analyzing the density of states (DOS) and molecular orbitals analysis [31]. Thus, the optical limiting behavior of PABA was accounted in the present paper.

2. Material and methods

2.1. Experimental details

PABA was purchased from TCI chemicals (https://www.tcichemicals.com/IN/en/) product number M0267 with >97% purity. All the spectroscopic calculations like absorbance and FT-IR have been performed using the compound as it is in deionized water without any further filtration. The solution of the PABA was prepared by mixing 5.485×10^{-3} g of PABA in 5 ml of deionized water to get the solution of PABA of concentration 5×10^{-3}M. Absorption and FT-IR were done using the same solution. Absorption spectra were recorded at 300 K with a Perkin-Elmer absorption spectrophotometer (model Lamda-35, source: tungsten iodide and deuterium) in the spectral range 200–1100 nm with a varying slit width (0.5 and 1.0 nm). The absorption spectra were further employed to obtain the band gap (Eg). Eg for PABA in water was depicted by plotting the Tauc plot defined using the Mott and Davis relation given below [32]:

$$(\alpha h\nu)^{\gamma} = A(h\nu - E_g) \tag{1}$$

Eg is the band gap, and γ is the constant that depicts the nature of the transitions (γ = 1/2, for direct allowed transitions called direct band gap). For the calculation of FT-IR spectra, a Perkin-Elmer FT-IR spectrophotometer (model Spectrum BX-II source: nichrome glower wire with DTGS detector) was used.

For the Z-scan experiment, a solution of PABA in concentration 2 mg/cm^3 was prepared in dimethyl formamide (DMF). The intensity-dependent open aperture Z-scan was performed using a 532 nm nano-pulsed Nd: YAG laser beam of 17 μm waist and 10 Hz frequency focused by the lens of 15 cm focal length. The third-order nonlinear absorption coefficient of the aqueous solution of the PABA sample was evaluated by the Z-scan experiment. The value of linear transmittance (L_T) was computed by Eq. (2) [33]:

$$L_T = \frac{P}{P_0} \tag{2}$$

P and P_0 are the values of the output power with and without samples. The value of the linear absorption coefficient (α_0) was computed using L_T and sample thickness L (1 mm) by Eq. (3) [34]:

$$\alpha_0 = -\left(\frac{1}{L}\right)\ln\left(\frac{P}{P_0}\right) \tag{3}$$

2.2. Computational details

The three-dimensional structure of PABA was downloaded from the online database PubChem (https://pubchem.ncbi.nlm.nih.gov/). All the quantum chemical calculations of the PABA in the water phase were done using Gaussian 09 (https://gaussian.com/glossary/g09/) software and the graphic user interface Gauss view (https://gaussian.com/gaussview6/) was used for the analysis of the results [35,36]. The ground state geometry optimization of PABA in the water was done using a restricted B3LYP/6-311G++(d,p) basis set with the scrf PCM model [37,38]. The optimized geometry of PABA was used to obtain the MEP surface and counterplots. The charge distribution of the PABA molecule was accounted by the Mulliken charge and natural charge distribution. The fingerprints of PABA were also examined by performing Hirshfeld's analysis by using Crystal Explorer software (https://crystalexplorer.net/) [39]. The inter-fragment charge transfer analysis (IFCT) was performed to for the quantitative study of the charge transfer and the local excitation of the charge cloud. The multiwfn (https://sobereva.com/multiwfn/) software packages were followed to perform the IFCT analysis [40]. The density of states (DOS) spectra was plotted to see the

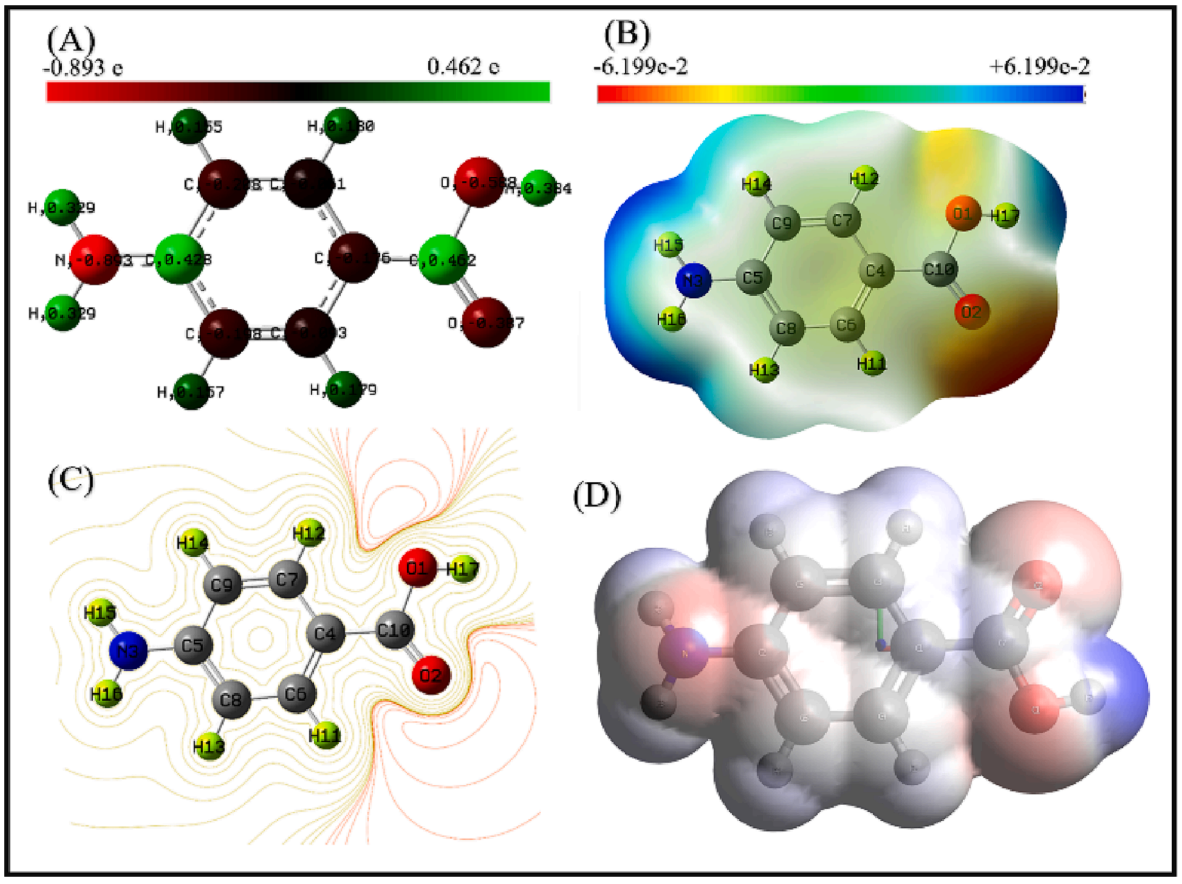

Fig. 1. (A) Optimized geometry of PABA computed by B3LYP/6-311G++(d,p) basis set with charge distribution, (B) MEP surface of PABA with potential range $\pm 6.199 \times 10^{-2}$ V, and active regions with red-color regions indicating the electron-withdrawing part, and blue indicating the electron-donating part of the title molecule, (C) counterplots of PABA, (D) Van der Waal surface of PABA showing red-colored regions with high ionization potentials and the blue-colored regions with low ionization potential.

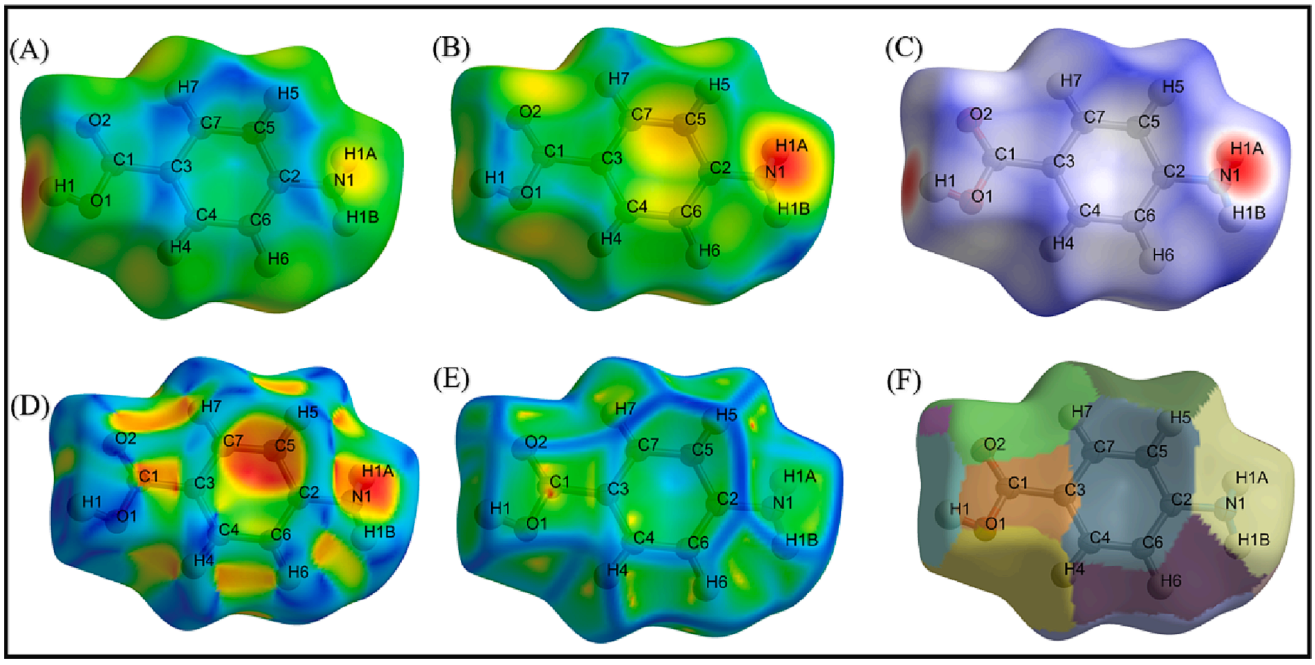

Fig. 2. Hirshfeld surfaces for (A) di (B) de (C) d norm (D) shape index (E) curvedness (F) fragment patch for PABA.

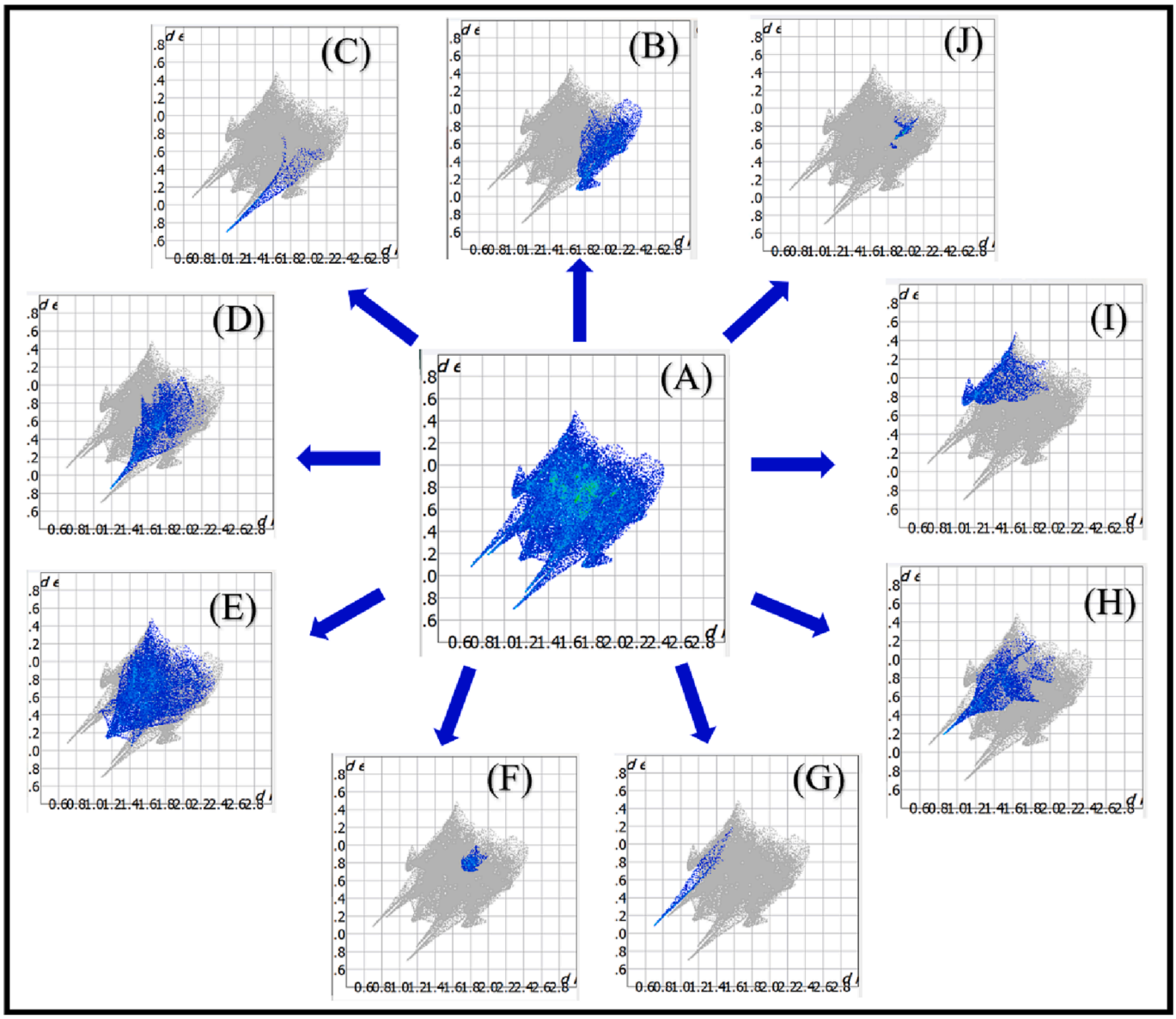

Fig. 3. Fingerprint plots of PABA for (A) overall PABA molecule, (B) C…H, (C) N…H, (D) O…H, (E) H…H, (F) C…C, (G) H…N, (H) H…O, (I) H…C, and (J) C…O.

corresponding energies of the HOMO and LUMO and the band gap. The DOS spectra was plotted using the Gauss Sum software (https://gausssum.sourceforge.net/) [41]. The simulated absorption was computed by time-dependent density functional theory (TD-DFT). The simulated FT-IR spectra of PABA in water were obtained by polar calculations. The experimental and simulated spectra were plotted using Origin software (https://www.originlab.com/). The NLO activity of the PABA in water was monitored by calculating the value of polarizability (α_{total}) and first-order hyperpolarizability (β_{total}) using Eqs. (4) and (5):

$$\alpha_{total} = \frac{1}{\sqrt{2}}\left[\left(\alpha_{xx}-\alpha_{yy}\right)^2+\left(\alpha_{yy}-\alpha_{zz}\right)^2+\left(\alpha_{zz}-\alpha_{xx}\right)^2+6\alpha_{xz}^2+6\alpha_{xy}^2+6\alpha_{yz}^2\right]^{\frac{1}{2}} \quad (4)$$

$$\beta_{total} = \left[\left(\beta_{xxx}+\beta_{xyy}+\beta_{xzz}\right)^2+\left(\beta_{yyy}+\beta_{yzz}+\beta_{yxx}\right)^2+\left(\beta_{zzz}+\beta_{zxx}+\beta_{zyy}\right)^2\right]^{\frac{1}{2}} \quad (5)$$

3. Results and discussion

3.1. Geometry and charge analysis

PABA has linear geometry with C1 point group symmetry with one amino (NH_2) and one carboxyl group (–COOH) attached to the ortho and para position of the benzene ring respectively. The dipole moment of 4.74 Debye was obtained in the gas phase after the ground state optimization of the PABA. The dipole moment of PABA increases to 6.58 Debye in the water. The bond length was higher (1.45 Å) for the 4C–10C bond that connects the carboxyl group to the benzene ring. The conjugated double bonds 5C=8C, 7C=9C, and 4C=6C have a high bond length of 1.41 Å. Conjugation plays a vital role in increasing the chemical reactivity of the compound. The conjugated bonds (alternate single and double bonds) enhance the availability of the free electron cloud for bond formation. The benzene ring conjugation thus shows the conjugated bonds participation in the charge transfer. The charge transfer was also observed in the Mulliken charge distribution shown in Fig. 1(A). The 1O and 2O have negative charges of −0.588 e and −0.387 e respectively whereas the 10C (0.462 e) and 17H (0.384 e) were

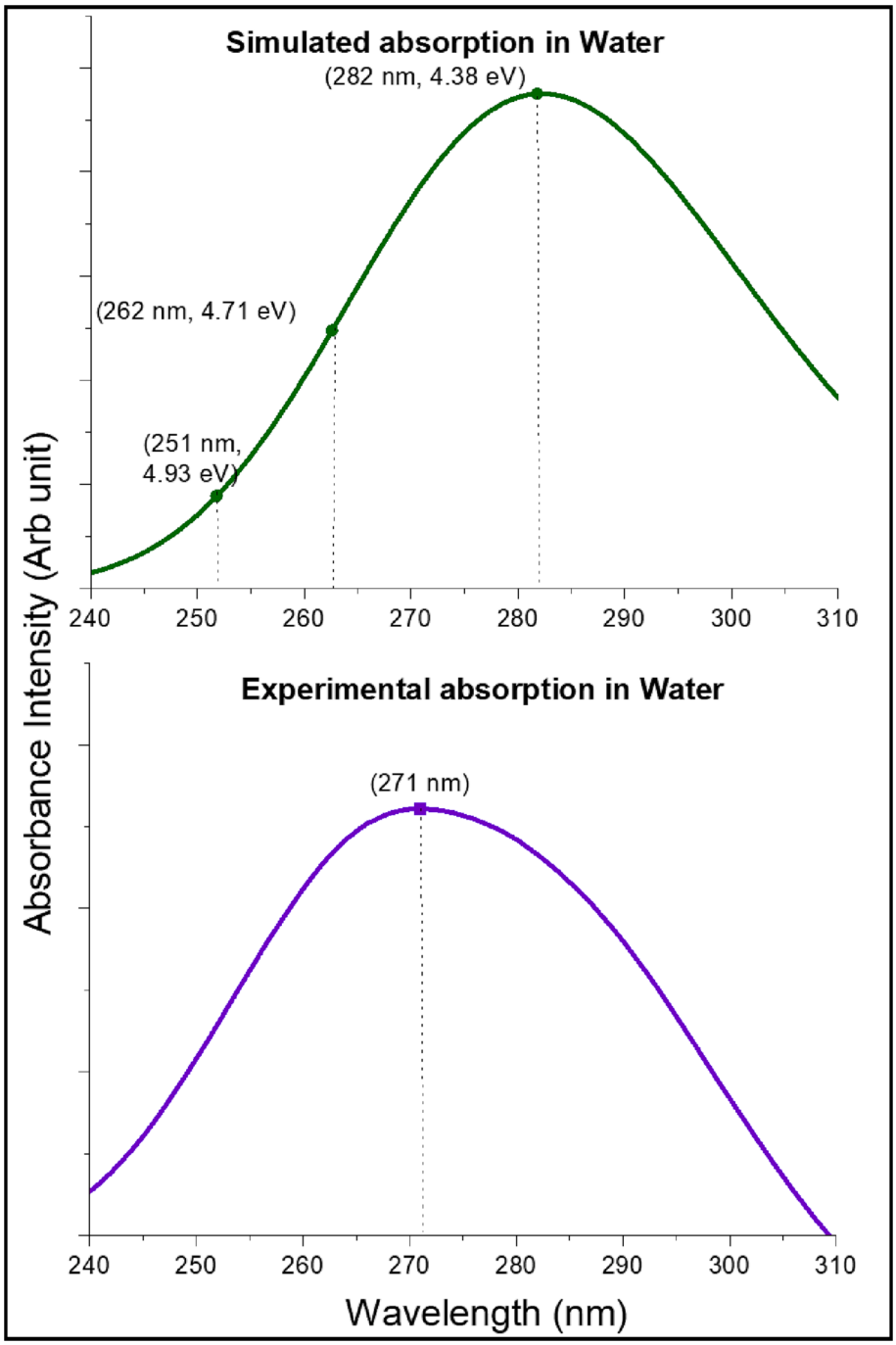

Fig. 4. (A) Simulated and (B) Experimental absorption spectra of PABA in water.

positively charged. Also, in the amino group, the 3N atom was negatively charged but the 15H and 16H hydrogen atoms of the amino group were positively charged. This shows the variation of the charge among the functional groups of PABA. The variation of the charges indicates the charge transfer between the amino and carboxyl groups. Moreover, the MEP surface indicates the active participation of the aforementioned functional groups in PABA. The blue color of the MEP surface indicates the regions with nucleophilic behavior and the red color surface over the oxygen atoms indicates the electrophilic nature of the PABA (Fig. 1(B)) [42]. The distribution of the electrophilic and nucleophilic surfaces indicates the charge transfer from the amino group toward the oxygen atoms of the carboxyl groups. Parallelly, highly accumulated counter lines around the carboxyl group in PABA indicate the collection of charge density around the carboxyl group (Fig. 1(C)). The counter plots indicate the regions that are highly influenced by the electric field. Such high charge accumulation was also supported by the ionization potential map. The Vander Waal surface illustrated in Fig. 1(D) shows the red-colored regions with high ionization potentials and the blue-colored regions with low ionization potential. The surface analysis indicates the intramolecular charge interactions between the amino and carbonyl groups.

3.2. *Hirshfeld and fingerprint plots analysis*

Hirshfeld surfaces were plotted for the PABA and shown in Fig. 2. Hirshfeld surfaces plotted over normalized contact distance (dnorm) are used to predict the intermolecular interactions [43]. The contact distances de and di are the distances from the Hirshfeld surface to the

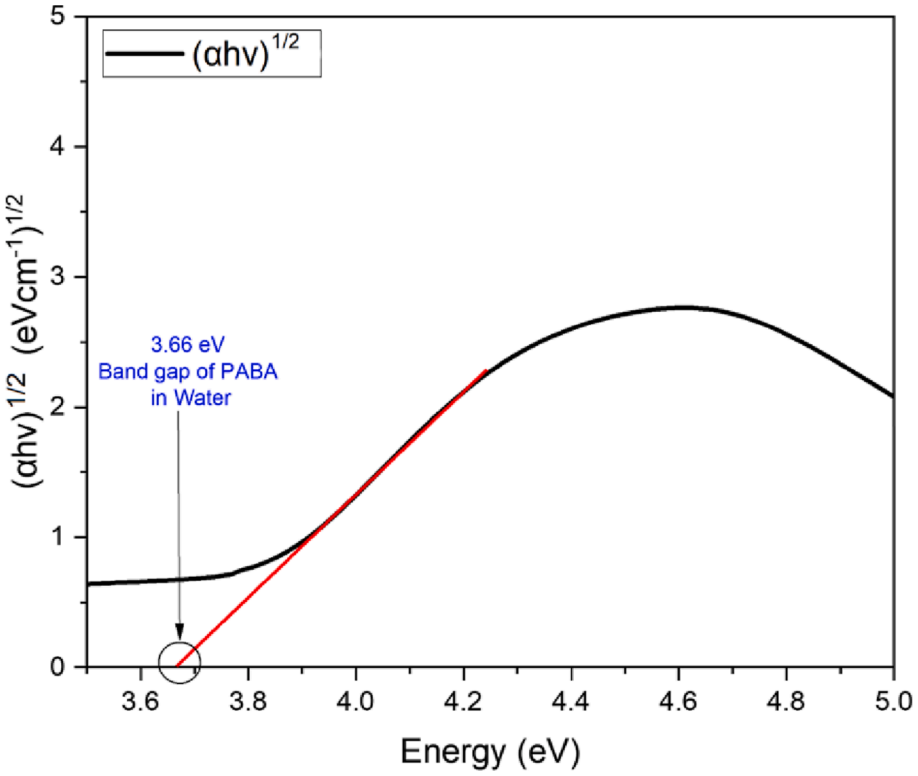

Fig. 5. Tauc plot from UV–Vis analysis of a PABA that illustrates the method of fitting the linear region to evaluate the band-gap at the X-axis intercept (3.66 eV).

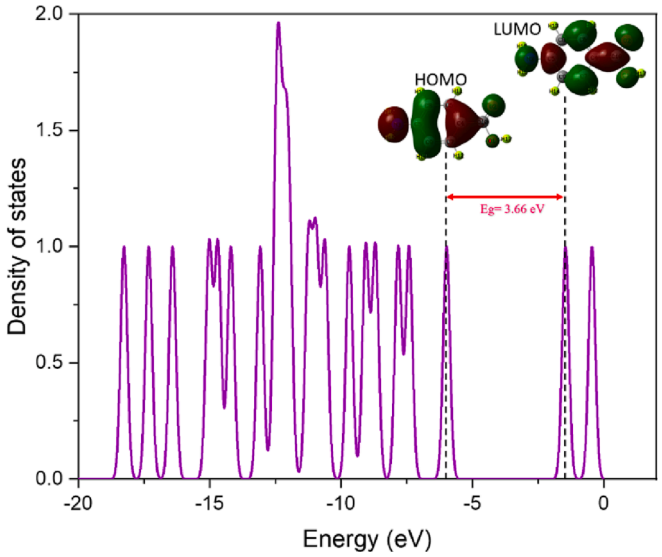

Fig. 6. Density of states plot of PABA with HOMO-LUMO surfaces.

nearest atoms outside and inside the surface, respectively. di, de, and dnorm were observed in the range ±2.47 Å, ±2.51 Å, and ±1.28 Å respectively. di and de surfaces indicate that the carboxyl group was the nearby bond to the Hirshfeld and the farthest bond from the Hirshfeld was an amino group (Fig. 2(A) and 2(B)). Dark red spots over the carboxyl and amino group visible in the dnorm surface is generally used for showing the activated moieties of the molecules to support the surface analysis done for locating the electron-donating and withdrawing agents of the PABA (Fig. 2(C)). The shape index (Fig. 2(D)), curvedness (Fig. 2(E)), and fragment path (Fig. 2(F)) were depicted in ranges ±1.00 Å, ±0.400 Å, and 0.00–13.00 Å respectively. These surfaces were in better agreement with the dnorm surface.

Table 1
Quantitative charge transfer and local excitation percentages and values of the PABA.

Charge contribution		Local excitation		
Atom	Charge	$S_0 \rightarrow S_1$ ($f = 0.4567$)		
Atom 1(O)	−0.46113082	36 → 37	H → L	95%
Atom 2(O)	−0.40194336	35 → 38	H-1 → L + 1	32%
Atom 3(N)	−0.30550056			
Atom 4(C)	−0.07167953	$S_0 \rightarrow S_2$ ($f = 0.0123$)		
Atom 5(C)	0.03970525	36 → 38	H → L + 1	70%
Atom 6(C)	−0.09596864	35 → 37	H-1 → L	27%
Atom 7(C)	−0.09742940			
Atom 8(C)	−0.14080245	$S_0 \rightarrow S_3$ ($f = 0.0001$)		
Atom 9(C)	−0.14122772	34 → 37	H-2 → L	96%
Atom 10(C)	0.36611546	35 → 38	H-1 → L + 1	32%
Atom 11(H)	0.12617698			
Atom 12(H)	0.12372620			
Atom 13(H)	0.11436128			
Atom 14(H)	0.11310778			
Atom 15(H)	0.22248576			
Atom 16(H)	0.22270909			
Atom 17(H)	0.38729472			

Fingerprint plots were plotted for the prediction of the percentage share of interatomic bonds in the intramolecular interactions. H…H interactions were seen to have the highest percentage of 36.5% (Fig. 3(E)) followed by C…H (15.6%) and O…H (14.5%) (Fig. 3(B) and 3(D)). A high percentage of H…H is due to 15H and 16H atoms attached to 3N. However, the 1O-17H bond of the –COOH group was the major reason behind the high percentage share in intramolecular interactions. It was observed that the nucleophilic bonds of PABA majorly contribute to the intramolecular interactions. This was in better agreement with the MEP surface. The 1O-17H bond acts as a nucleophilic moiety. C…O, N…H, H…N, and C…C interactions have low contributions of 1.4%, 3%, 2.8%, and 2.5% respectively in the total intramolecular interactions in PABA.

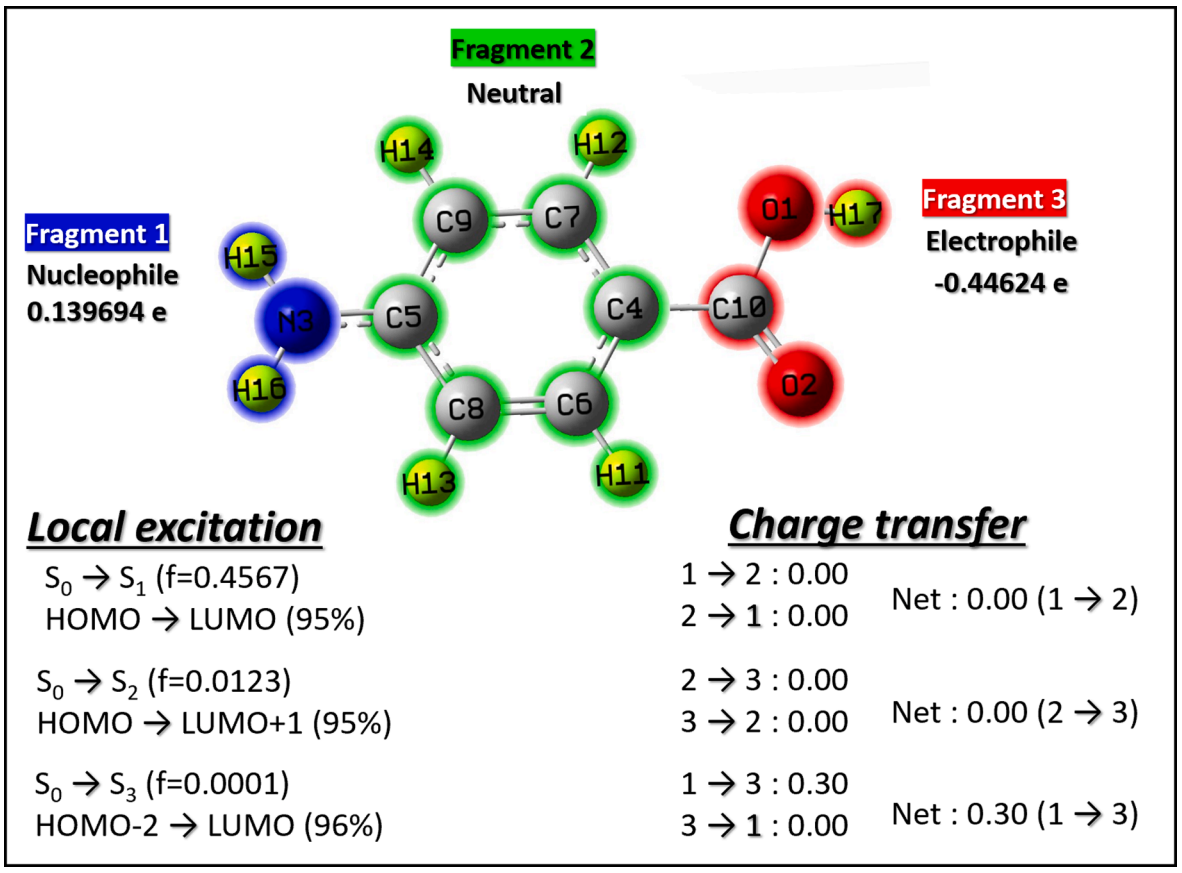

Fig. 7. Charge transfer and local excitation among the three fragments of the PABA molecule highlighted by colors. Blue-nucleophilic, green-neutral, and red-electrophilic.

Table 2
Computed values of μ_{total}, α_{total}, and β_{total} for PABA, and reference compounds urea, phenyl urea, and thiourea (all values are in esu).

Molecule	μ_{total}	α_{total}	β_{total}	*Reference*
PABA	6.58	18.42×10^{-24}	29.99×10^{-30}	–
Urea	1.52	6.30×10^{-24}	0.16×10^{-30}	[52]
Phenyl urea	4.2	15.19×10^{-24}	2.12×10^{-30}	[53]
Thiourea	5.49	7.79×10^{-24}	0.88×10^{-30}	[54]

Apart from the decomposition analysis, there found two distinct spikes of equal lengths in 2D plots for di and de each. The outer peaks (Fig. 3(C) and 3(G)) were mainly observed due to the N….H/H…N contributors which are donating peaks of the plots. On the other side, the inner two peaks (Fig. 3(D) and 3(H)) of di and de each correspond to O…H/H…O interactions. These O…H/H…O interactions are the contributions from the 10C=2O of the carboxyl group that acts as an electron-withdrawing agent of PABA. Thus, the Hirshfeld analysis identified that the nucleophilic parts of the PABA are dominant contributors to the Vander Waal interactions and hydrogen bonding in the PABA molecule.

3.3. Absorption and bandgap analysis

The electronic transitions were monitored using experimental and simulated absorption spectra for PABA. One broad absorption band was observed for both simulated and experimental spectra for PABA in the wavelength range of 240 to 310 nm (Fig. 4). The peak of simulated absorption spectra was observed at 282 nm with an oscillator strength of 0.58 and excitation energy of 4.38 eV. The experimental absorption for the sample of PABA has a lower cut-off wavelength at the UV region (271 nm) with the highest absorbance intensity, which is assigned transition $S_0 \rightarrow S_1$ as the π–π* transition [44]. The band gap was depicted by plotting the Tauc plot (Fig. 5) for PABA between $(\alpha h\nu)^{1/2}$ $(eVcm^{-1})^{1/2}$ and energy. The value of the direct band gap for PABA was observed as 3.66 eV. The low-cut-off wavelength at the UV region and wide optical bandgap suggest that PABA could be used for optoelectronics applications.

3.4. Molecular orbitals analysis

The DOS of PABA was studied to account for the accumulation of the highest occupied and lowest unoccupied (HOMO-LUMO) orbitals [45]. The DOS spectra of PABA are illustrated in Fig. 6. The HOMO peaks were more than the LUMO peaks. The high accumulation of the HOMO peaks justified the availability of the large charge cloud over the HOMO. The computed band gap obtained in DOS spectra (3.66 eV) was found to be equivalent to the band gap obtained by the Tauc plot by experimental absorption spectra. This better supports the obtained computational results. For a better understanding of the transferring of the charge cloud, the HOMO-LUMO surfaces have been shown in DOS spectra. The green and red colored surfaces over the geometry of PABA are HOMO-LUMO surfaces. The green surface is over the atoms that have excessive electrons and acts as electron-donating while the red surfaces cover the moieties with a lack of charge cloud and behaves as electron-withdrawing moieties [46,47] It was observed that the red surface over the amino group in HOMO is shifted over the conjugated C-C bonds of the benzene ring in LUMO and the red surface over C-C bond get shifted towards the amino group. This shifting of the surface illustrates that charge is being transferred from the amino group. Also, the green surface over the carboxyl group is smaller in HOMO and the size increases in LUMO. This shows the increased charge cloud over the

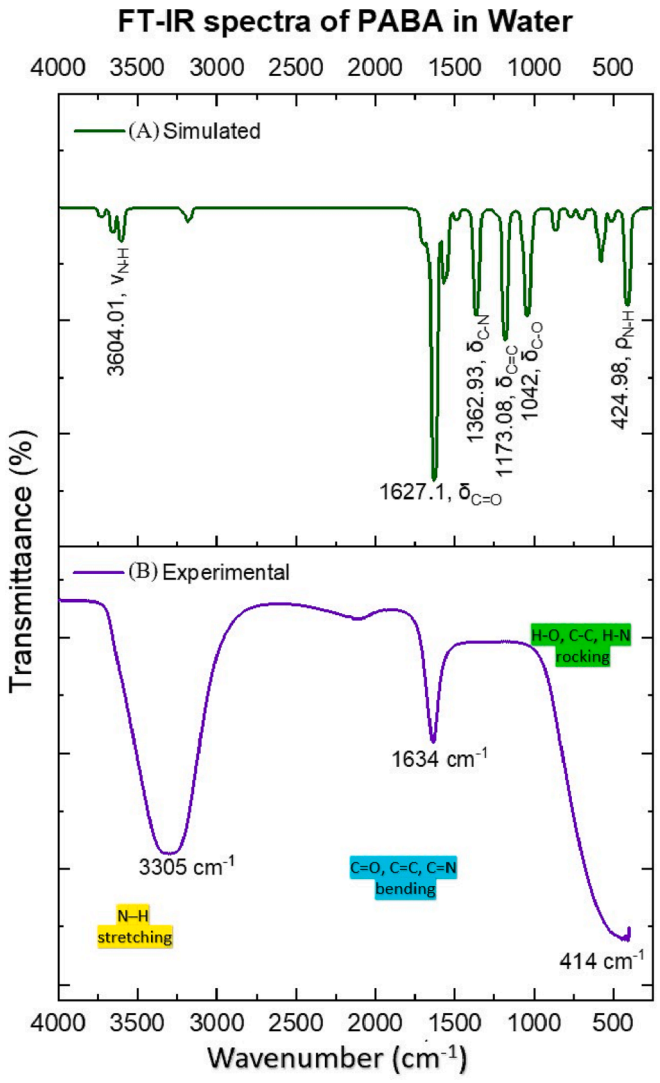

Fig. 8. (A) Simulated and (B) Experimental FT-IR spectra of PABA in water.

carboxyl group. Thus, the HOMO-LUMO surfaces demonstrated the shifting of the charge cloud from the amino group toward the carboxyl group. This interpretation also corresponds to the statement drawn from the MEP surfaces. So, DOS spectra and HOMO-LUMO surfaces confirm the path of the charge dislocation and the nature of intramolecular interactions within PABA.

3.5. Inter-fragment charge transfer analysis

The IFCT analysis is the method that is used to quantitatively measure the exact amount of charge that is transferred from the nucleophilic toward the electrophilic moieties [48,49]. The PABA is divided into three fragments dividing the nucleophile (say, 3N, 15H, and 16H), electrophile (1O, 2O, 10C, 17H) and the neutral (4C, …9C; 11H, …14H) fragment. The local excitation modes $S_0 \rightarrow S_1$, S_2, S_3 were recorded and the details of all the transitions with local excitation percentages are listed in Table 1. Among the local excitation transitions listed in Table 1, the $S_0 \rightarrow S_1$ have the highest oscillator strength of 0.4567 with two distinguished excitations between HOMO to LUMO, and HOMO-1 to LUMO+1. These excitations have a local excitation percentage of 95% and 32% respectively. On the other hand, the charge transfer analysis done by the IFCT process reveals that 0.139694 e and −0.44624 e charges were possessed by fragment 1 and fragment 3. The total charge transfer measured between the fragments was mentioned in Fig. 7. No charge transfer was observed between fragments 1 & 2, and 2 & 3. It was observed that a 0.30 e charge was transferred from fragment 1 to fragment 3. This was 23% of the total charge of fragment 1 that was seen to be dislocated from nucleophilic towards electrophilic fragments. The charge transfer percentage was comparatively lower than the local excitation percentage in PABA. Thus, from the IFCT analysis, the charge interactions were found to be due to the local excitation of the charge. Table 2.

3.6. Vibrational analysis

FT-IR spectra were obtained for the title molecule experimentally as well as computationally. The vibrational modes were obtained to get a better idea and understanding of the modes undergoing high vibrations and the nature of vibrations [50]. The simulated FT-IR spectra of PABA illustrated in Fig. 8(A) were obtained in water using B3LYP/6-311G++(d,p) basis set in polar calculations and the experimental FT-IR spectra obtained for the water solution of PABA with a 0.5 M concentration is illustrated in Fig. 8(B). The higher frequency modes tend to impart the polarizability of the molecules which is a key to NLO characteristics. Both the simulated and experimental spectra reflected major vibrational modes for the bonds of amino and carboxyl groups. The linear symmetric stretching (ν_{NH}) of the 3N – 15H and 3N – 16H bonds was the mode having the highest frequency of 3604.01 cm^{-1}. Similar N – H bond modes were observed in experimental spectra around 3305 cm^{-1}. Amino and carbonyl groups were the main functional groups that leads to the ICT in PABA. Both computed and experimental FT-IR gave prominent vibrational peaks for amino and carbonyl groups. The highest frequency modes for the amino group were observed with the highest intensity around 3000–3500 cm^{-1}. The carbonyl group was observed to give bending modes nearby 1600 cm^{-1}. One sharp peak for the torsional bending (δ_{CO}) of the 10C=2O and 10C–1O was obtained in simulated spectra at 1627 cm^{-1}. In experimental FT-IR, the same kind of sharp peak for the bending of the carboxyl group was observed at 1634 cm^{-1}. Various peaks for the bending of C=O and C=C bonds were observed in the range of 500–1500 cm^{-1}. The rocking of the N – H bonds of the amino group exists at 424 cm^{-1} in simulation spectra and at 414 cm^{-1} in experimental spectra. Thus, high peaks in the FT-IR spectra gave high peaks for the stretching and bending of the functional groups. Therefore, it can be stated that the stretching and bending of the functional groups were majorly responsible for the high polarizability of the PABA. Additionally, the simulated and experimental spectra seem to harmonize at the peaks.

3.7. Hyperpolarizability analysis

Dipole moment (μ_{total}), linear polarizability (α_{total}), and hyperpolarizability (β_{total}) are the parameters that mainly comment on the linear and NLO behavior of any compound. Generally, the μ_{total} is the parameter by which one can get an idea about the varying electronegativities of any compound. The larger the difference between the electronegativities of the associated atoms, the larger will be the intramolecular charge interactions and the larger will be the optical nonlinearity of the molecule [51]. The value of μ_{total} was calculated as 6.58 Debye for PABA in water. These values are four times higher than Urea (1.52 Debye), double that of phenyl urea (4.2 Debye), and comparatively higher than Thiourea (5.49 Debye). Thus, it can be stated that PABA has better availability of large diffused electron clouds than urea, thiourea, and phenyl urea. α_{total} for PABA was calculated as 18.429×10^{-24} esu. β_{total} is the higher-order expansion of magnetic susceptibility that defines the optical non-linearity of the compound. The β_{total} of PABA was computed around 29.99×10^{-30} esu. The β_{total} of PABA was found much higher than reference compounds. These values are 187 times higher than Urea (0.16×10^{-30} esu), fifteen times higher than phenyl urea (2.12×10^{-30} esu), and 34 times higher than thiourea (0.88×10^{-30} esu). Thus, the hyperpolarizability analysis reveals that

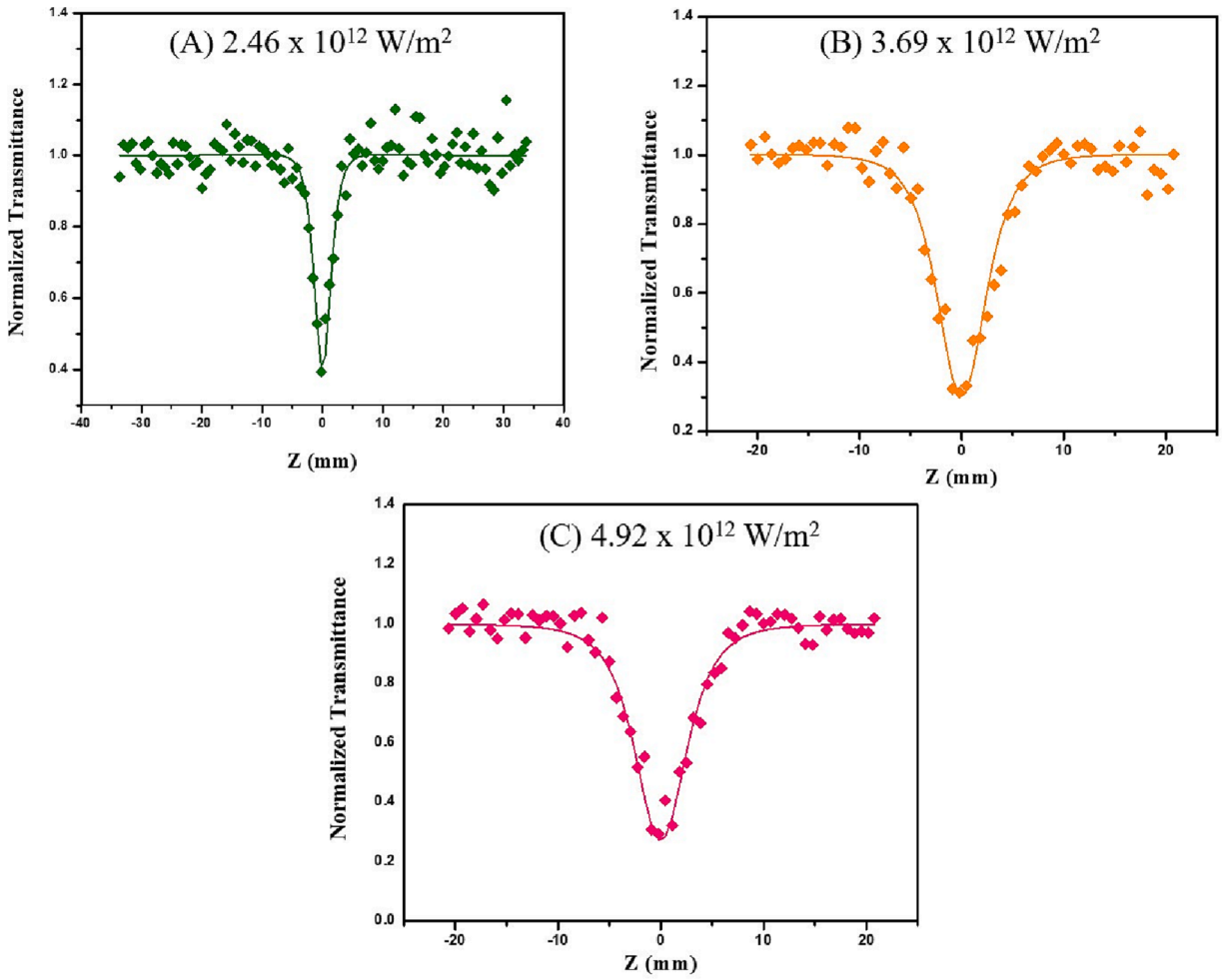

Fig. 9. Intensity-dependent Open-aperture Z-scan pattern of PABA using Nd-ÝAG nano pulsed laser (532 nm and pulse energy – 100 μJ) for intensity (A) 2.46 × 10^{12} W/m^2, (B) 3.69 × 10^{12} W/m^2, and (C) 4.92 × 10^{12} W/m^2.

PABA has the better potential to be employed as NLO material.

3.8. Z-Scan analysis

An open aperture Z-scan experiment performed for varying intensities of 2.46 × 10^{12} W/m^2, 3.69 × 10^{12} W/m^2, and 4.92 × 10^{12} W/m^2 are illustrated in Fig. 9. Two different kinds of signatures of the Z-scan experiment are possible, one with a sharp peak at the focus and one with a valley-like inverted peak at the focus [55]. The former shows saturable absorption (SA) while the latter indicates reverse saturable absorption (RSA) in the sample [56]. RSA means that the transmittance decreases with the increase of excitation laser power [57]. Additionally, the compound with SA has a negative value of nonlinear absorption coefficients (β) while the compound with RSA has a positive value of β [58]. As shown in Fig. 9, a valley-shaped curve symmetric about the focal (Z = 0) axes represents the reverse saturable absorption nature of PABA. The experimental Z-scan data were fitted theoretically to understand the nature of the nonlinear absorption. Using Sheik-Bahae formalism, the normalized transmittance of the PABA was computed using by the Eq. (6)

$$\frac{dI}{dz'} = \left[\frac{\alpha_0}{1+\frac{I}{I_s}} + \beta I\right] I \tag{6}$$

where α_0 is unsaturated linear absorption at the excitation, I is input intensity laser, I_s is saturation intensity, β is the effective coefficient of two-photon absorption (nonlinear absorption coefficient), Z is samples propagation distance. The value of the linear absorption coefficient was calculated as 3.147 cm^{-1}. The linear transmittance of PABA was computed as 0.73. Here the experimental data was found to be best fitting for the two-photon absorption (2PA) equation. As discussed in absorption and molecular orbital analysis, PABA possesses its absorption maxima in the ultraviolet region at 271 nm (4.58 eV). This π–π* transition of PABA avails the 2PA state and provides the chances of two-photon absorption. During green laser excitation, the PABA molecule either undergoes genuine two-photon absorption in which simultaneous absorption of two photons takes place, or sequential two-photon absorption where one photon absorption is followed by excited state absorption. As the Z-scan experiment cannot distinguish genuine and sequential 2PA processes, an intensity-dependent Z-scan experiment was performed. For different pulse energy of 100, 150, and 200 μJ, the two-photon absorption coefficient of PABA was found as 0.76, 0.85, and 1.20 × 10^{-10} m/W respectively. The values of β for all the samples are positive and arise due to the two-photon absorption process. As the 2PA coefficient is increasing with on-axis intensity, PABA exhibits sequential two-photon absorption (one-photon absorption followed by excited state absorption). Thus, PABA possesses the property of RSA arising from excited state absorption is involved in two-photon absorption.

3.9. Optical limiting behavior

The optical limiting behavior of PABA was established by plotting

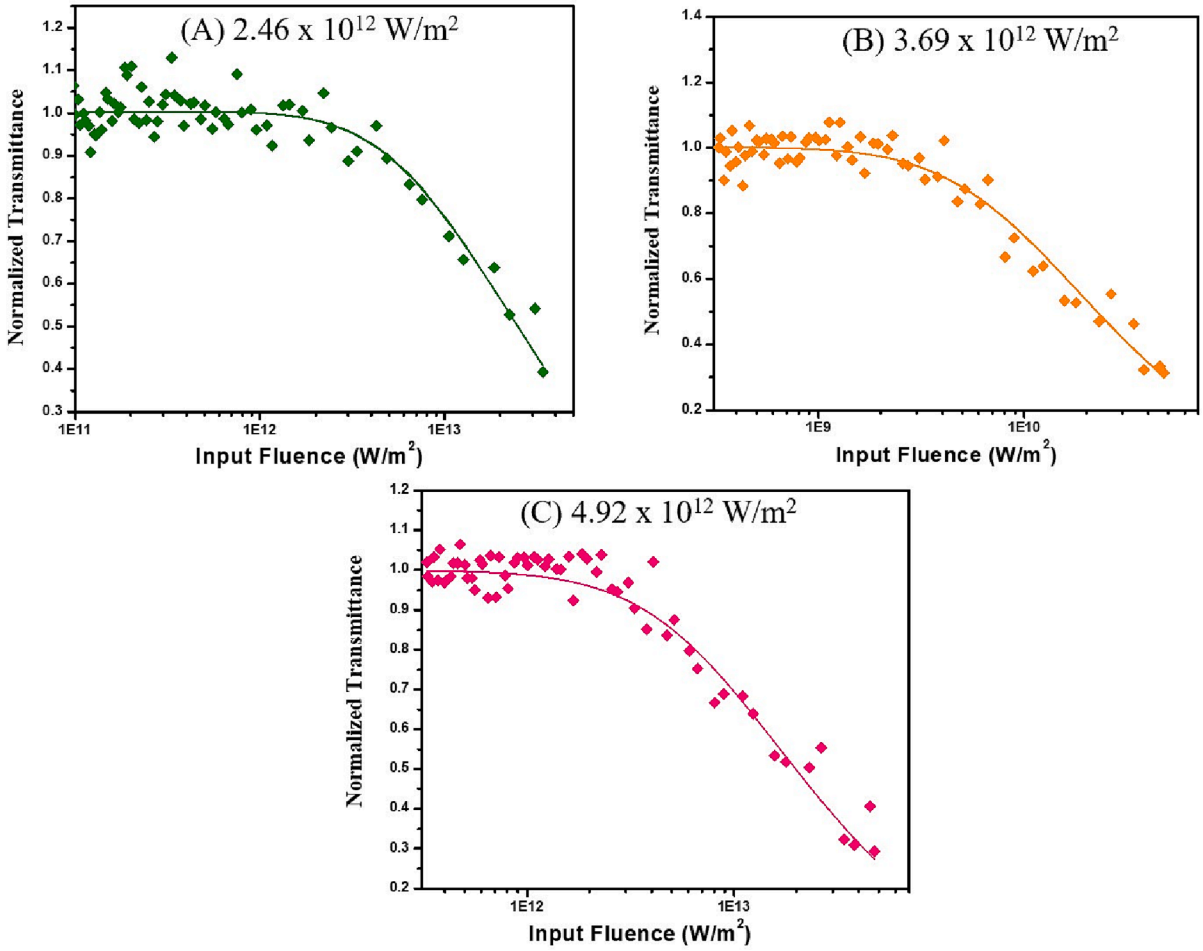

Fig. 10. Optical limiting graph of PABA for intensity (A) 2.46 × 10^{12} W/m^2, (B) 3.69 × 10^{12} W/m^2, and (C) 4.92 × 10^{12} W/m^2.

Table 3
Values of nonlinear absorption coefficient and optical limiting threshold for PABA.

Excitation Pulse Energy (μJ)	Saturation Intensity (×10^{11} W/m^2)	Nonlinear Absorption Coefficient β (×10^{-10} m/W)	Optical Limiting Threshold (×10^{13} W/m^2)
100	40	0.76	2.24
150	40	0.85	2.12
200	40	1.20	1.64

the optical limiting graph between normalized transmittance and input fluence. The optical limiting graph for three different intensities 2.46 × 10^{12} W/m^2, 3.69 × 10^{12} W/m^2, and 4.92 × 10^{12} W/m^2 was traced and shown in Fig. 10. It was observed that the value of normalized transmittance gradually decreases with an increase in input laser fluence and thus deviates from its linear pattern. So PABA exhibits optical limiting behavior arising from the two-photon absorption process. The value of the optical limiting threshold was found to be 2.24, 2.12, and 1.64 × 10^{13} W/m^2 for a pulse energy of 100, 150, and 200 μJ respectively (Table 3). Here the value of the optical limiting threshold was found to be decreased with increasing pulse energy showing the strengthening of optical limiting behavior. The optical limiting parameters of PABA were compared to some experimentally proven compounds with good laser damage threshold. The comparison was done between different benzoic acid derivatives and other organic laser limiting materials. The values of β of PABA was found better than all the considered reference compounds except urea picrate. Moreover, the optical limiting threshold of the PABA was found higher than all the considered compounds except L-

Table 4
Comparison of the nonlinear absorption coefficient, optical limiting threshold, and linear transmittance of PABA with other reference NLO compounds with proven optical limiting properties.

Compound	Nonlinear Absorption Coefficient β(×10^{-10} m/W)	Optical Limiting Threshold (×10^{13} W/m^2)	Linear Transmittance (%)	Reference
2-amino-4,6-dimethylpyrimidine benzoic acid	–	1.5	–	[22]
2-(2-methoxybenzyllideneamino)-5-methylphenylmercuric chloride	0.67	0.62	–	[59]
urea picrate	2.146	–	50	[60]
Isonicotinamide bis-p-aminobenzoic acid		0.57	58	[23]
L-Methionine Barium Bromide	0.17	0.82	80	[61]
L-phenylalanine–benzoic acid	–	6.5	85	[24]

Methionine Barium Bromide that have 0.82 × 10^{13} W/m^2. The linear transmittance of PABA was also found higher for some materials like urea picrate and Isonicotinamide bis-p-aminobenzoic acid, and comparable to L-Methionine Barium Bromide and L-phenylalanine–benzoic acid. Thus, the comparison mentioned in Table 4 indicates the potential optical limiting characteristics of PABA. Therefore, it can be stated that the PABA has the active ability to be employed as laser-blocking material and can act as an optical limiter towards the development of laser safety devices.

4. Conclusion

In the present work, the NLO activity of the PABA was reported by using experimental as well as computational tools. The DFT was used to establish the mechanism of the intramolecular interactions of PABA. The structural parameters showed that the bonds associated with the amino and the carboxyl group were seen to impart in the charge transfer. The location of the red and blue electrostatic potential surface over the carboxyl and amino groups of PABA reflected the accepting and donating nature of the functional groups respectively. Moreover, Hirshfeld's surfaces supported the interpretation of the MEP surface well. The fingerprint plots of different interactions of PABA were also found maximum for the N….H/H…N and O…H/H…O interactions. A strong absorption peak was observed for PABA in the visible region experimentally as well as computationally with a direct band gap of 3.66 eV computed by the Tauc plot and DOS spectra respectively. Higher vibrational peaks were obtained for the bonds of the functional groups in FT-IR spectra. The value of hyperpolarizability for PABA was found much higher than the reference compounds like Urea, phenyl urea, and thiourea. The deep valley-like inverted peak observed in Z-scan traces with the positive values of the nonlinear absorption coefficient showed the occurrence of reverse saturable absorption in the PABA solution. The theoretical fit confirms the observed RSA arises due to the two-photon absorption process. Moreover, the deviated optical limiting graphs strongly establish the optical limiting nature of PABA. Thus, it can be said that PABA possesses strong NLO responses and have an excellent ability to be used as an optical limiter for laser damage control applications.

CRediT authorship contribution statement

Shradha Lakhera: Writing – original draft, Visualization, Validation, Software, Investigation, Data curation. **Meenakshi Rana:** Writing – review & editing, Visualization, Supervision, Methodology, Conceptualization. **Kamal Devlal:** Writing – review & editing, Conceptualization. **Shruti Sharma:** Investigation. **Papia Chowdhury:** Visualization, Supervision, Resources. **Vivek Dhuliya:** Writing – original draft, Software, Investigation. **Sagar Panwar:** Investigation. **L.P. Purohit:** Visualization, Supervision, Resources. **A. Dhanusha:** Visualization, Validation, Investigation. **T.C. Sabari Girisun:** Investigation, Resources, Supervision, Visualization.

Declaration of Competing Interest

The authors declare that they have no known competing financial interests or personal relationships that could have appeared to influence the work reported in this paper.

Data availability

No data was used for the research described in the article.

References

[1] F. Ullah, N. Kosar, A. Ali, M.T. Mahmood, K. Ayub, Alkaline earth metal decorated phosphide nanoclusters for potential applications as high performance NLO materials; A first principle study, Phys. E: Low-Dimens. Syst. Nanostruct. 118 (2020) 113906. https://doi.org/10.1016/j.physe.2019.113906.
[2] M. Rana, N. Singla, A. Pathak, A. Dhanya, C. Narayana, P. Chowdhury, Vibrational-electronic properties of intra/inter molecular hydrogen bonded heterocyclic dimer: An experimental and theoretical study of pyrrole-2-carboxaldehyde, Vib. Spectrosc 89 (2017) 16–25, https://doi.org/10.1016/j.vibspec.2016.12.003.
[3] M.S. Al-Buriahi, V.P. Singh, H. Arslan, V.V. Awasarmol, B.T. Tonguc, Gamma-ray attenuation properties of some NLO materials: potential use in dosimetry, Radiat. Environ. Biophys. 59 (1) (2020) 145–150, https://doi.org/10.1007/s00411-019-00824-y.
[4] V. Krishnakumar, R. Nagalakshmi, Studies on the first-order hyperpolarizability and terahertz generation in 3-nitroaniline, Phys. B Condens. Matter 403 (10) (2008) 1863–1869, https://doi.org/10.1016/j.physb.2007.10.341.
[5] S. Munsif, S. Khan, A. Ali, M.A. Gilani, J. Iqbal, R. Ludwig, K. Ayub, Remarkable nonlinear optical response of alkali metal doped aluminum phosphide and boron phosphide nanoclusters, J. Mol. Liq. 271 (2018) 51–64, https://doi.org/10.1016/j.molliq.2018.08.121.
[6] A. Özarslan, D. Çakmaz, F. Erol, H. Şenöz, N. Seferoğlu, A. Barsella, Z. Seferoğlu, Synthesis and investigation of photophysical, NLO and thermal properties of D-π-A-π-D dyes, J. Mol. Struct. 1229 (2021) 129583, https://doi.org/10.1016/j.molstruc.2020.129583.
[7] D. Marappan, M. Palanisamy, S.H. Mon, B. Babu, C. Sivakumar, Growth, vibrational, optical, mechanical and DFT investigations of an organic nonlinear optical material – phenylurea, Z. Phys. Chem. 233 (2019) 1659–1682, https://doi.org/10.1515/zpch-2018-1230.
[8] S. Lakhera, K. Devlal, M. Rana, V. Dhuliya, N. Pandey, Non-linear optical behavior of 2,9-dimethylquinacridone with adsorbed gold and silver nanoclusters, Optik (2023) 170983, https://doi.org/10.1016/j.ijleo.2023.170983.
[9] S. Lakhera, K. Devlal, M. Rana, Investigation of the electronic and optical activity of halogen-substituted 2-nitrotoulene by density functional theory, Opt. Quant. Electron. 55 (2023) 292, https://doi.org/10.1007/s11082-023-04569-3.
[10] S. Lakhera, M. Rana, K. Devlal, Investigation of nonlinear optical responses of organic derivative of imidazole: imidazole-2-carboxaldehyde, IJMR (2023), https://doi.org/10.1515/ijmr-2021-8649.
[11] S. Lakhera, K. Devlal, A. Ghosh, M. Rana, In silico investigation of phytoconstituents of medicinal herb 'Piper Longum' against SARS-CoV-2 by molecular docking and molecular dynamics analysis. 3 (2021) 100199. https://doi.org/10.1016/j.rechem.2021.100199.
[12] Q. Cheng, X. Shi, C. Li, Y. Jiang, Z. Shi, J. Zou, X. Wang, X. Wang, Z. Cui, Chromophores with side isolate groups and applications in improving the poling efficiency of second non-linear optical (NLO) materials, Dyes Pigm. 162 (2019) 721–727, https://doi.org/10.1016/j.dyepig.2018.11.001.
[13] S.T. Lee, W.M. Khairul, O.J. Lee, R. Rahamathullah, A.I. Daud, K. Halim, K. Bulat, S. Sapari, F.I.A. Razak, G. Krishnan, Electronic, reactivity and third order nonlinear optical properties of thermally-stable push-pull chalcones for optoelectronic interest: Experimental and DFT assessments, J. Phys. Chem. Solid 159 (2021) 159, https://doi.org/10.1016/j.jpcs.2021.110276.
[14] S. Lakhera, K. Devlal, M. Rana, V. Dhuliya, Quantum mechanical study of three aromatic bioactive fatty alcohol compounds with nonlinear optical and potential light harvesting properties, Opt. Mat. 129 (2022), 112476, https://doi.org/10.1016/j.optmat.2022.112476.
[15] S. Lakhera, M. Rana, K. Devlal, I. Celik, R. Yadav, A comprehensive exploration of pharmacological properties, bioactivities and inhibitory potentiality of luteolin from Tridax procumbens as anticancer drug by in-silico approach, Struct. Chem. (2022), https://doi.org/10.1007/s11224-022-01882-7.
[16] M. Rana, N. Singla, A. Chatterjee, A. Shukla, P. Chowdhury, Investigation of nonlinear optical (NLO) properties by charge transfer contributions of amine functionalized tetraphenylethylene, Opt. Mater. 62 (2016) 80–89, https://doi.org/10.1016/j.optmat.2016.09.043.
[17] S. Lakhera, M. Rana, K. Devlal, Theoretical study on spectral and optical properties of essential amino acids: a comparative study, Opt. Quant. Electron. 54 (2022) 714, https://doi.org/10.1007/s11082-022-04118-4.
[18] M. Sheikhi, S. Shahab, R. Alnajjar, M. Ahmadianarog, Adsorption properties of the new anti-cancer drug alectinib on CNT (6,6-6) nanotube: geometry optimization, molecular structure, spectroscopic (NMR, UV/Vis, Excited State), FMO, MEP and HOMO–LUMO investigations, J. Clust. Sci. 30 (2019) 83–96, https://doi.org/10.1007/s10876-018-1460-9.
[19] T. Vasanthi, V. Balasubramanian, V.N. Vijayakumar, Theoretical studies (DFT) on hydrogen bonded liquid crystal derived from 4-amino and 4-dodecyloxy benzoic acids, Mater. Today:. Proc. 47 (2021) 1724–1730, https://doi.org/10.1016/j.matpr.2021.01.900.
[20] J. George, V. Sasikala, L.K. Joy, D. Sajan, T. Arumanayagam, P. Murugakoothan, G. Vinitha, Vibrational spectra, dielectric properties, conductivity mechanisms and third order nonlinear optical properties of guanidinium 4-aminobenzoate, Opt. Mater. 89 (2019) 48–62, https://doi.org/10.1016/j.optmat.2019.01.006.
[21] V. Arunachalam, B. Vidyavathy, G. Vinitha, Structure and characterization of a new organic crystal for optical limiting applications, isonicotinamide bis-p-aminobenzoic acid. https://doi.org/10.3116/16091833/17/2/98/2016.
[22] B.S.I. Lasalle, P. Karuppasamy, M.S. Pandian, P. Ramasamy, Investigation of structural, optical, and thermal properties of 2-amino-4,6-dimethylpyrimidine benzoic acid (2APB) single crystal for non-linear optical (NLO) applications, J. Mater. Sci. Mater. Electron. 33 (22) (2022) 17780–17792, https://doi.org/10.1007/s10854-022-08643-6.
[23] M. Andreea, M. Maria, C. Catalin, I. Valentin, M. Bogdana, I. Iulian, D. Maria, E. Ana, Nonlinear optical studies on 4-(ferrocenylmethylimino)-2-hydroxy-benzoic acid thin films deposited by matrix-assisted pulsed laser evaporation (MAPLE),

Appl. Surf. Sci. 374 (2016) 206–212, https://doi.org/10.1016/j.apsusc.2015.11.024.
[24] S. Tamilselvan, M. Vimalan, I. Vetha Potheher, S. Rajasekar, R. Jeyasekaran, M. Antony Arockiaraj, J. Madhavan, Growth, thermal, dielectric and mechanical properties of L-phenylalanine–benzoic acid: A nonlinear optical single crystal, SAA 114 (2013) 19–26, https://doi.org/10.1016/j.saa.2013.05.017.
[25] T. Bharanidharan, A. Senthil, S. Ranjith, Synthesis, crystal growth, structural and physicochemical properties of N-methylurea benzoic acid single crystal for non-linear optical applications, J. Mol. Struct. 1281 (2023), 135136, https://doi.org/10.1016/j.molstruc.2023.135136.
[26] P. Karuppasamy, T. Kamlesh, V. Mohankumar, S. Kalam, Abdul, M. Pandian, S. Muthu, P. Ramasamy, S. Verma, S. Rao, S. Venugopal, Synthesis, growth, structural, optical, thermal, laser damage threshold and computational perspectives of 4-nitrophenol 4-aminobenzoic acid monohydrate (4NPABA) single crystal. J. Mol. Struct. (2018), S0022286018310238. https://doi.org/10.1016/j.molstruc.2018.08.074.
[27] S. Janani, Hemamalini Rajagopal, S. Muthu, S. Aayisha, M. Raja, Molecular structure, spectroscopic (FT-IR, FT-Raman, NMR), HOMO-LUMO, chemical reactivity, AIM, ELF, LOL and Molecular docking studies on 1-Benzyl-4-(N-Boc-amino)piperidine. J. Mol. Struct. 1230 (2021) 129657. https://doi.org/10.1016/j.molstruc.2020.129657.
[28] F.B. Rizwana, S. Muthu, J.C. Prasana, C.S. Abraham, M. Raja, Spectroscopic (FT-IR, FT-Raman) investigation, topology (ESP, ELF, LOL) analyses, charge transfer excitation and molecular docking (dengue, HCV) studies on ribavirin, CDC 17–18 (2018) 236–250, https://doi.org/10.1016/j.cdc.2018.09.003.
[29] R.S. Saji, J.C. Prasana, S. Muthu, J. George, T.K. Kuruvilla, B.R. Raajaraman, Spectroscopic and quantum computational study on naproxen sodium, Spectrochim. Acta A 226 (2020), 117614, https://doi.org/10.1016/j.saa.2019.117614.
[30] P. Jayaprakash, P. Sangeetha, M. Peer Mohamed, G. Vinitha, S. Muthu, M. Prakash, M. Lydia Caroline, Growth and characterization of dl-Mandelic acid (C6H5CH(OH) CO2H) single crystal for third-order nonlinear optical applications, J. Mol. Struct. 1148 (2017) 314–321, https://doi.org/10.1016/j.molstruc.2017.07.049.
[31] P. Manjusha, J.C. Prasana, S. Muthu, B.F. Rizwana, Spectroscopic elucidation (FT-IR, FT-Raman and UV-visible) with NBO, NLO, ELF, LOL, drug likeness and molecular docking analysis on 1-(2-ethylsulfonylethyl)-2-methyl-5-nitro-imidazole: An antiprotozoal agent, CBAC. 88 (2020), 107330, https://doi.org/10.1016/j.compbiolchem.2020.107330.
[32] J. Singh, Electronic processes in amorphous semiconductors. J. Mater. Sci.: Mater. Electron. 14 (2003) 171–186 (2003). https://doi.org/10.1023/A:1022310108978.
[33] T.C. Sabari Girisun, S. Dhanuskodi, Nonlinear optical susceptibilities of diglycinyl thiourea for frequency conversion and optical limiting applications, Chem. Phys. Lett. 491 (4-6) (2010) 248–253, https://doi.org/10.1016/j.cplett.2010.04.014.
[34] S.S. Shinde, M.C. Sreenath, S. Chitrambalam, I.H. Joe, N. Sekar, Spectroscopic, DFT and Z-scan approach to study linear and nonlinear optical properties of Disperse Red 277, Opt. Mater. 99 (2020), 109536, https://doi.org/10.1016/j.optmat.2019.109536.
[35] M. J. Frisch, G. W. Trucks, H. B. Schlegel, et al., Gaussian 09, Revision B. 01, Gaussian Inc., Wallingford CT. 121 (2009) 150-166.
[36] R. Dennington, T. Keith, J. Millam, GaussView, Version 4.1.2, Semichem, Inc., Shawnee Mission, KS (2007).
[37] A.D. Becke, Density-functional thermochemistry. III. The role of exact exchange, J. Chem. Phys. 98 (1993) 5648, https://doi.org/10.1063/1.464913.
[38] A.D. Becke, Density-functional thermochemistry. V. Systematic optimization of exchange-correlation functionals, J. Chem. Phys. 107 (1997) 8554–8560, https://doi.org/10.1063/1.475007.
[39] P.R. Spackman, M.J. Turner, J.J. McKinnon, S.K. Wolff, D.J. Grimwood, D. Jayatilaka, M.A. Spackman, CrystalExplorer: a program for Hirshfeld surface analysis, visualization and quantitative analysis of molecular crystals, J. Appl. Cryst. 54 (3) (2021) 1006–1011, https://doi.org/10.1107/S1600576721002910.
[40] L.u. Tian, F. Chen, Multiwfn, J. Comput. Chem. 33 (2012) 580–592.
[41] N.M. O'Boyle, A.L. Tenderholt, K.M. Langner, J. Comp. Chem. 29 (2008) 839–845.
[42] S. Lakhera, K. Devlal, A. Ghosh, P. Chowdhury, M. Rana, Modelling the DFT structural and reactivity study of feverfew and evaluation of its potential antiviral activity against COVID-19 using molecular docking and MD simulations, Chem. Pap. 76 (5) (2022) 2759–2776, https://doi.org/10.1007/s11696-022-02067-6.
[43] Y.S. Mary, Y.S. Mary, A.S. Rad, R. Yadav, I. Celik, S. Sarala, Theoretical investigation on the reactive and interaction properties of sorafenib – DFT, AIM, spectroscopic and Hirshfeld analysis, docking and dynamics simulation, J. Mol. Liq. 330 (2021), 115652, https://doi.org/10.1016/j.molliq.2021.115652.
[44] S. Lakhera, K. Devlal, M. Rana, I. Celik, Study of nonlinear optical responses of phytochemicals of Clitoria ternatea by quantum mechanical approach and investigation of their anti-Alzheimer activity with in silico approach, Struct. Chem. (2022), https://doi.org/10.1007/s11224-022-01981-5.
[45] M. Saranya, S. Ayyappana, R. Nithya, R.K. Sangeetha, A. Gokila, Molecular structure, nbo and homo-lumo analysis of quercetin on single layer graphene by density functional theory, Dig. J. Nanomater. Biostruct. 13 (2018) 97–105.
[46] S. Lakhera, M. Rana, K. Devlal, N. Kanagathara, J. Janczak, Photovoltaic characteristics of organic heterocyclic 2,9-dimethyl quinacridone in different solvents using DFT approach, J. Photochem. Photobiol. A Chem. 441 (2023) 114664, https://doi.org/10.1016/j.jphotochem.2023.114664.
[47] S. Lakhera, K. Devlal, M. Rana, V. Dhuliya, Computational study of non-linear optical and electrical properties of 1,3-dinitropyrene, Opt. Quant. Electron. 55 (2023) 85, https://doi.org/10.1007/s11082-022-04371-7.
[48] Karatay, A. et al., Amino-functionalized nitrogen-doped graphene quantum dots and silver-graphene based nanocomposites: Ultrafast charge transfer and a proof-of-concept study for bioimaging applications, J. Photochem. Photobiol. A. 426 (2022) 113741. https://doi.org/10.1016/j.jphotochem.2021.113741.
[49] E. A. Yildiz, et al., Effects of heavy iodine atoms and π-expanded conjugation on charge transfer dynamics in carboxylic acid BODIPY derivatives as triplet photosensitizers. Chem. Phys. Chem. 24 (2023) e202200735 https://doi.org/10.1002/cphc.202200735.
[50] T. Hema, P. Bhatt, C. Arya, H. Dhondiyal, K. Tiwari, Devlal, Structural and vibrational study of molecular interaction in a ternary liquid mixture of benzylamine, ethanol and benzene, Struct. Chem. (2021), https://doi.org/10.21203/rs.3.rs-649250/v1.
[51] S. Lakhera, M. Rana, K. Devlal, Influence of adsorption of gold and silver nanoclusters on structural, electronic, and nonlinear optical properties of pentacene-5, 12-dione: A DFT study, Opt. Quant. Electron. 55 (2023) 178, https://doi.org/10.1007/s11082-022-04422-z.
[52] Z. Lin, Z. Wang, C. Chen, M.-H. Lee, Mechanism of linear and nonlinear optical effects of KDP and urea crystals Citation, J. Chem. Phys. 118 (5) (2003) 2349–2356, https://doi.org/10.1063/1.1533734.
[53] D. Marappan, M. Palanisamy, M.S. Ho, B. Babu, S. Chandrasekar, V. Growth, Optical, mechanical and DFT investigations of an organic nonlinear optical material – phenylurea, Z. Phys. Chem. 233 (11) (2019) 1659–1682, https://doi.org/10.1515/zpch-2018-1230.
[54] O. L. Santos, T. L. Fonseca, J. R. Sabino, H. C. Georg, M. A. Castro, Polarization effects on the electric properties of urea and thiourea molecules in solid phase. J. Chem. Phys. 143 (2015) 234503. https://doi.org/10.1063/1.4937481.
[55] J. Sarrato, A.L. Pinto, G. Malta, E.G. Röck, J. Pina, J.C. Lima, A.J. Parola, P. S. Branco, New 3-ethynylaryl coumarin-based dyes for DSSC applications: synthesis, spectroscopic properties, and theoretical calculations, Molecules 26 (2021) 2934, https://doi.org/10.3390/molecules26102934.
[56] T.C. Sabari Girisun, S. Dhanuskodi, G. Vinitha, χ(3) measurement and optical limiting properties of metal complexes of thiourea using Z-scan, Mater. Chem. Phys. 129 (1–2) (2011) 9–14, https://doi.org/10.1016/j.matchemphys.2011.04.013.
[57] P. Vani, G. Vinitha, K.A. Naseer, K. Marimuthu, M. Durairaj, T.C. Sabari Girisun, N. Manikandan, Thulium-doped barium tellurite glasses: structural, thermal, linear, and non-linear optical investigations, J. Mater. Sci. Mater. Electron. 32 (10) (2021) 1–17, https://doi.org/10.1007/s10854-021-06787-5.
[58] A. Pramothkumara, N. Senthilkumarb, R. Mary Jenilac, M. Durairaj, T.C. Sabari Girisund, I.V. Pothehera, A study on the electrical, magnetic and optical limiting behaviour of Pure and Cd-Fe co-doped CuO NPs, J. Alloy. Compd. 878 (2021), 160332, https://doi.org/10.1016/j.jallcom.2021.160332.
[59] H.Q.M. Ali, Two-photon absorption-based optical limiting in 2-(2-methoxybenzyllideneamino)-5-methylphenylmercuric chloride-doped PMMA film, Mod. Phys. Lett. B 28 (10) (2014), 1450079, https://doi.org/10.1142/s0217984914500791.
[60] K. Naseema, M. Shyma, K.B. Manjunatha, A. Muralidharan, G. Umesh, V. Rao, χ(3) measurement and optical limiting studies of urea picrate, Opt. Laser Technol. 43 (7) (2011) 1286–1291, https://doi.org/10.1016/j.optlastec.2011.03.025.
[61] M. Shalini, R.S. Sundararajan, E. Manikandan, M. Meena, B. Samuel Ebinezer, T. C. Sabari Girisun, R. Natarajan, Growth and characterization of L - Methionine Barium Bromide (LMBB) semi-organic crystal for optical limiting applications, Optik 278 (2023), 170705, https://doi.org/10.1016/j.ijleo.2023.170705.